ADVANCED SCIENCE Open Access
www.advancedscience.com

Promoted Growth and Multiband Emission in Heterostructured Perovskites Through Cs^+-Sublattice Interaction

Lei Zhou, Liangliang Liang, Jiaye Chen, Xin Zhou, Lingmei Liu, Shibo Xi, Kian Ping Loh, Yu Han, Qian He,* and Xiaogang Liu**

Precise control of exciton confinement in metal halide perovskites is critical to the development of high-performance, stable optoelectronic devices. A significant hurdle is the swift completion of ionic metathesis reactions, often within seconds, making consistent control challenging. Herein, the introduction of different steric hindrances in a Cs^+ sublattice within $CsYb_2F_7$ is reported, which effectively modulates the reaction rate of Cs^+ with lead (Pb^{2+}) and halide ions in solution, extending the synthesis time for perovskite nanostructures to tens of minutes. Importantly, the Cs^+ sublattice provides a crystal facet-dependent preference for perovskite growth and thus exciton confinement, allowing the simultaneous occurrence of up to six emission bands of $CsPbBr_3$. Moreover, the rigid $CsYb_2F_7$ nano template offers high activation energy and enhances the stability of the resulting perovskite nanostructures. This methodology provides a versatile approach to synthesizing functional heterostructures. Its robustness is demonstrated by in-situ growth of perovskite nanostructures on Cs^+-mediated metal-organic frameworks.

1. Introduction

Metal-halide perovskite quantum dots (MHP QDs) have gained prominence in recent years because of their exceptional optical and electronic properties, including high luminescence quantum yield, narrow emission bandwidth, and tunable luminescence.[1] However, the ionic nature of these compounds also poses several challenges to their synthesis and applications.[2] Specifically, the nucleation and growth of MHP QDs occur too quickly through rapid ionic metathesis reactions, making it difficult to control with conventional hot injection or precipitation techniques. This poses a major obstacle to controlling the exciton confinement of QDs and a fundamental understanding of their nucleation, growth kinetics, and especially luminescence mechanisms.[3] Despite enormous efforts, it remains challenging

L. Zhou, L. Liang, J. Chen, K. P. Loh, X. Liu
Department of Chemistry
National University of Singapore
Singapore 117549, Singapore
E-mail: ifellliang@xmu.edu.cn; chmlx@nus.edu.sg
L. Zhou
School of Chemical Engineering and Technology
Sun Yat-sen University
Zhuhai 519802, P. R. China
X. Zhou, Q. He
Materials Science and Engineering
National University of Singapore
Singapore 117575, Singapore
E-mail: mseheq@nus.edu.sg
L. Liu
Multi-scale Porous Materials Center
Institute of Advanced Interdisciplinary Studies & School of Chemistry and Chemical Engineering Chongqing University
Chongqing 400044, P. R. China
S. Xi
Institute of Sustainability for Chemicals
Energy and Environment (ISCE2)
Agency for Science, Technology and Research (A*STAR)
1 Pesek Road Jurong Island, Singapore 627833, Singapore
Y. Han
Physical Sciences and Engineering Division
Advanced Membranes and Porous Materials (AMPM) Center
King Abdullah University of Science and Technology (KAUST)
Thuwal 23955–6900, Saudi Arabia
X. Liu
Institute of Materials Research and Engineering
Agency for Science, Technology and Research
Singapore 138634, Singapore
X. Liu
The N1 Institute for Health
National University of Singapore
Singapore 117456, Singapore

The ORCID identification number(s) for the author(s) of this article can be found under https://doi.org/10.1002/advs.202306398

DOI: 10.1002/advs.202306398

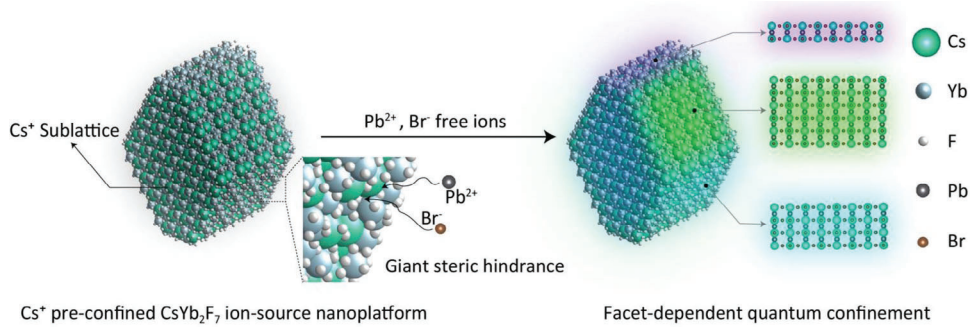

Figure 1. Controlling exciton confinement in lead halide perovskites using a Cs^+-preconfined nanoplatform. The enrichment of Cs^+ ions in a robust crystalline framework provides a distinct steric hindrance, leading to a marked slowdown of the perovskite synthesis. The varied exposure of the Cs^+ sublattice across distinct facets of the $CsYb_2F_7$ nanoplatform leads to facet-dependent perovskite reconstruction and thus to significant variations in the exciton confinement of perovskite nanostructures.

to contain the rapid growth of MHP QDs to achieve controlled exciton confinement.[4] Unlike the widely used approach of using catalysts to lower the activation energy and thereby expedite organic synthesis, the introduction of steric hindrances can increase the activation energy and thus decelerate the reaction.[5] Although surface engineering through ligands has proven effective in controlling the synthesis kinetics of perovskite QDs, organic ligands offer only a moderate steric hindrance.[6]

Herein, we speculate that incorporating Cs^+ ions into a rigid nanocrystal lattice might substantially reduce their reactivity toward other ions in solution, allowing subsequent control of the kinetics of perovskite growth on the surface. Moreover, the multifaceted nature of the selected nanocrystal matrix offers varied reaction environments, leading to facet-specific reaction kinetics on a single nanoplatform. We reason that a rationally designed Cs^+-sublattice nanoplatform will allow perovskite nanostructures to be tailored from multilayers down to molecular dimensions, thereby achieving refined exciton confinement (**Figure 1**). On a Cs^+-sublattice nanoplatform, we can observe fluorescence emissions stemming from various exciton confinements. In addition, the inherent rigidity of the Cs^+-sublattice suggests that the resulting perovskite nanostructures may exhibit enhanced stability.

2. Results and Discussion

Alkali metal-lanthanide fluorides are the most popular host materials for the development of highly stable luminescent nanomaterials.[7] Using the co-precipitation method,[8] we synthesized $CsYb_2F_7$ nanoparticles at 290 °C, which serve as Cs^+-preconfined nanocrystals for perovskite synthesis. These nanocrystals have a diameter of about 10 nm and are linked to oleic acid (OA) ligands at the surface (**Figure 2A**; Figure S1, and

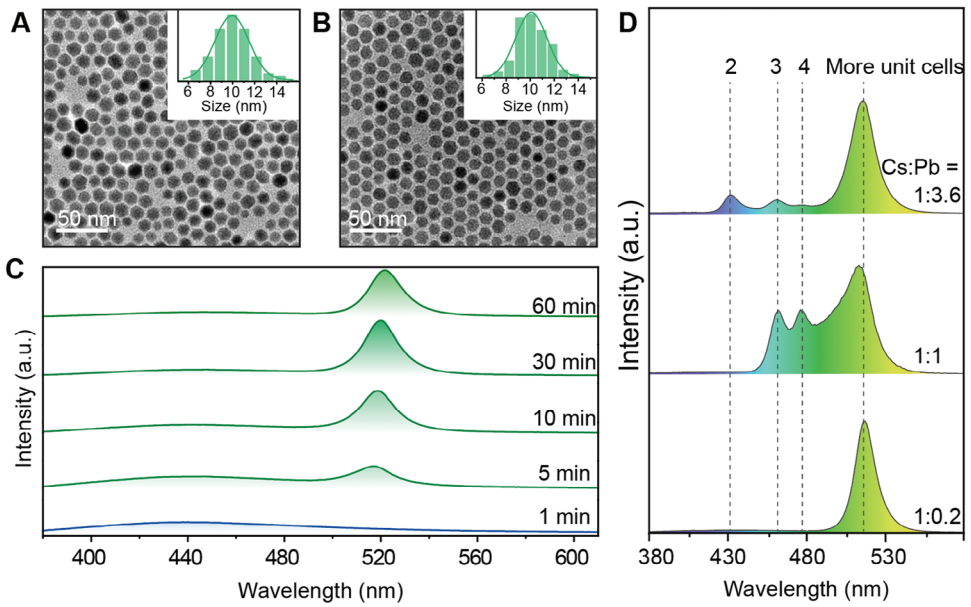

Figure 2. Lead halide perovskite synthesis and spectra tuning on a sub-10 nm $CsYb_2F_7$ nanoplatform. A,B) Transmission electron micrographs of $CsYb_2F_7$ nanocrystals: pristine A) and post-reaction B) with Pb^{2+} and Br^- ions. Insets show the corresponding size distributions. C) Emission spectra from $CsYb_2F_7/CsPbBr_3$ at varying reaction durations, maintaining a 1:0.2 molar ratio of Cs^+ to Pb^{2+}. D) Emission spectra of the prepared $CsYb_2F_7/CsPbBr_3$ products after 30 min of reaction at various Cs^+-to-Pb^{2+} ratios (1:0.2, 1:1, and 1:3.6).

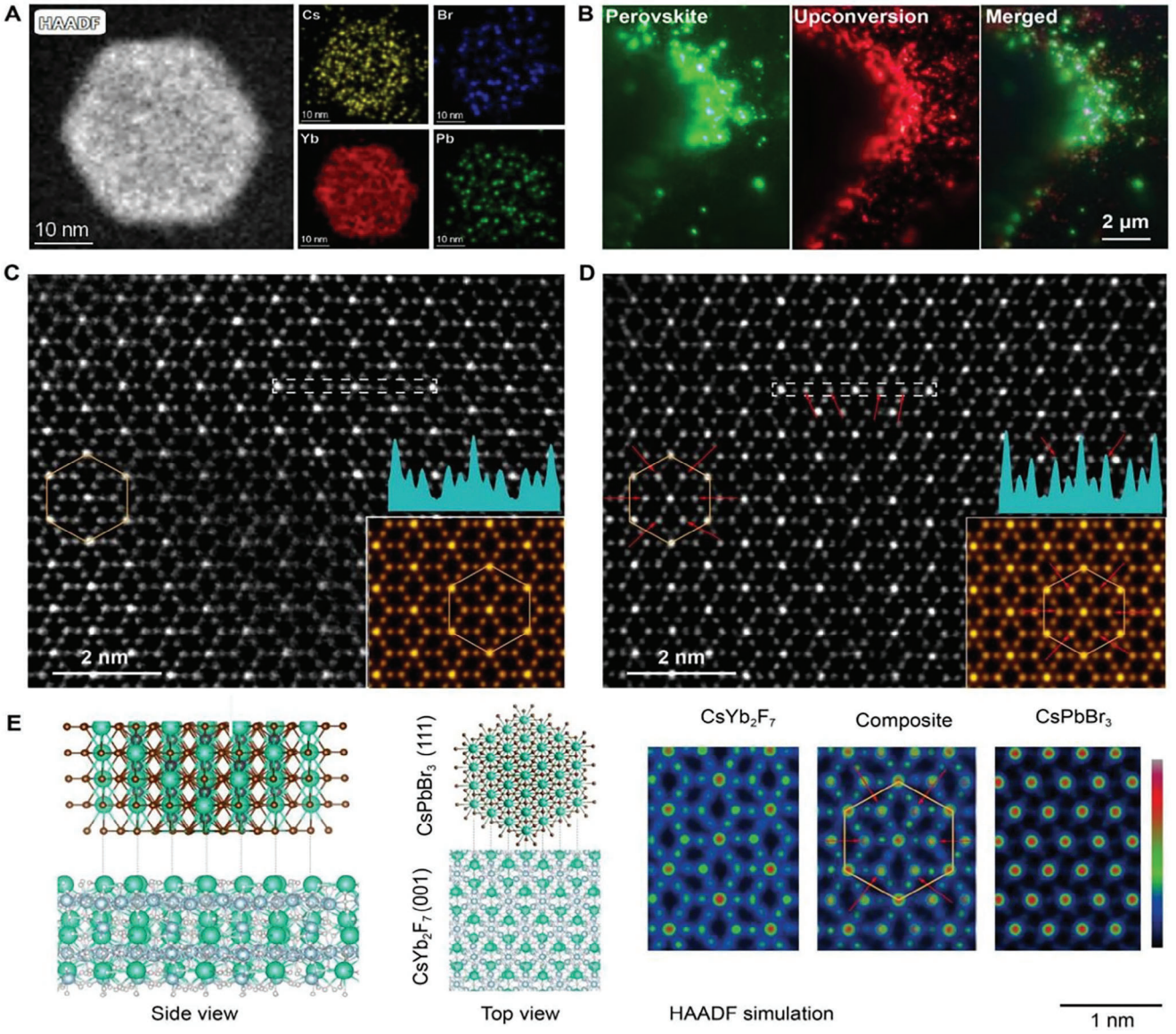

Figure 3. Structural investigation of lead-halide perovskite nanostructures constructed on $CsYb_2F_7$ nanoplates. A) High-angle annular dark field (HAADF) scanning transmission electron microscopy (STEM) image of a $CsYb_2F_7$ nanoplate after reaction and the corresponding elemental mapping (Cs^+, Br^-, Yb^{3+}, and Pb^{2+}). B) Optical micrographs of 2% Er^{3+}-doped $CsYb_2F_7$ nanoplates after reaction: under 365 nm excitation (left), 980 nm excitation (middle), and the merged image (right). C,D) HAADF-STEM images of the $CsYb_2F_7$ platform and the $CsYb_2F_7$/$CsPbBr_3$ composite. The inset shows the corresponding atomic arrangement from the inverse Fourier transform. E) Crystal structure of the $CsYb_2F_7$ nanoplatform and the $CsPbBr_3$ perovskite in side view and top view. The right panel shows the HAADF simulation in top view for the (001) facet of $CsYb_2F_7$, the (111) facet of $CsPbBr_3$, and their heterostructural composite.

Table S1, Supporting Information). A solution containing $PbBr_2$ dissolved in OA, oleylamine (OAm), and 1-octadecene (ODE) was used for the subsequent growth of lead-halide perovskites on the surface of as-prepared $CsYb_2F_7$ nanocrystals. As the solution was injected at 180 °C for five minutes, green emission was observed under ultraviolet irradiation, which became brighter over time. Note that no additional Cs^+ ions are introduced to the solvent, and the exclusive source of Cs^+ ions is $CsYb_2F_7$ nanocrystals. The following chemical reaction equation might partially represent the synthesis process, as the inner part of $CsYb_2F_7$ is not participating in the reaction:

$$3PbBr_2+2CsYb_2F_7 \rightarrow 2CsPbBr_3+4Yb^{3+}+14F^-+Pb^{2+} \quad (1)$$

While general perovskite synthesis can be completed rapidly, the development of green emissions on the $CsYb_2F_7$ nanoplatform takes much longer, with a plateau being reached after 30 min following injection (Figure 2B,C; Figure S2, Supporting Information). Moreover, the $CsYb_2F_7$ nanoplatform showed negligible changes in morphology after reaction (Figure 2B and Figure S3, Supporting Information). Although $CsPbBr_3$ nanostructures formed on $CsYb_2F_7$ exhibited a spectral blue shift and had comparable lifetimes with standard $CsPbBr_3$ quantum

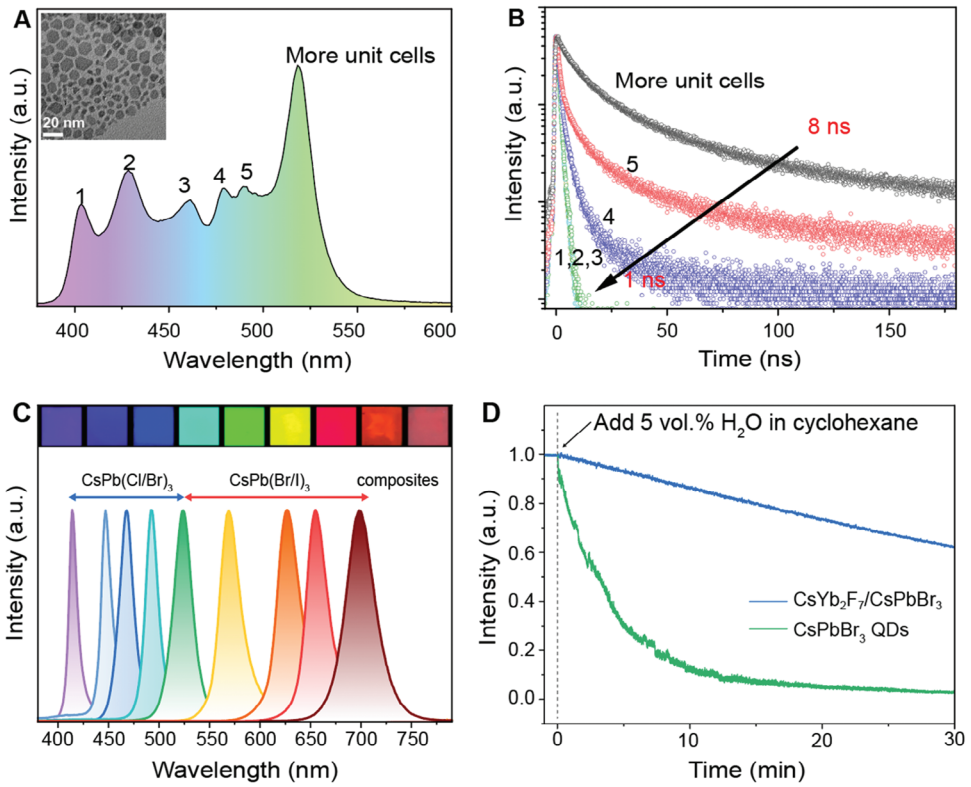

Figure 4. Cs^{+}-confined nanoplatform for the synthesis of lead halide perovskites with tunable luminescence. A) The emission spectrum of $CsPbBr_3$ grown on $CsYb_2F_7$ nanoplates with low homogeneity, showing six transition bands. B) The variation of lifetime (from 8 to 1 ns) of the six transition emissions (from 517 to 402 nm) under 365 nm excitation. C) Emission spectra and corresponding photographs of perovskites prepared on nanorod templates with varied halogens. D) A stability comparison between conventional $CsPbBr_3$ quantum dots and their counterparts developed on $CsYb_2F_7$ nanoplatforms.

dots (Figure S4–S6, Supporting Information), no distinguishable X-ray diffraction (XRD) peaks corresponding to $CsPbBr_3$ were observed from the emitting nanoplatforms (Figure S7, Supporting Information). These results imply that the observed green emission is from few-layer perovskites without notable Bragg diffraction. Meanwhile, Fourier-transform infrared spectroscopy results confirmed the presence of oleamine on the surface of $CsYb_2F_7/CsPbBr_3$ (Figure S8, Supporting Information). Intriguingly, when the initial molar ratio of Pb^{2+} to Cs^{+} confined in $CsYb_2F_7$ was increased, multiple emission bands with fixed peak positions emerged at shorter wavelength regions (Figure 2D). Since Br^{-} ions are the only halogens used, the emergence of these blue-shifted emission peaks can be attributed to different degrees of exciton confinements.[9] Therefore, the $CsYb_2F_7$ nanoplatform may provide a growth preference for lead-halide perovskites that depends on the exposed facets.

Given that a specific crystal facet on a sub-10 nm nanoplatform has a small surface area and is susceptible to drifting and decomposition under electron beams, we synthesized a larger plate-like $CsYb_2F_7$:Er^{3+}(2%) nanoplatform (30 nm in diameter) that predominantly exposes the (001) facet for perovskite synthesis and structural investigation (**Figure 3A** and Figure S9, Supporting Information). By co-doping Er^{3+} into $CsYb_2F_7$ nanoplates, strong red upconversion emission was observed in response to laser pumping at 980 nm, facilitating identification with an optical microscope. After the reaction, elements such as Cs, Yb, Pb, and Br can be identified in a single nanoplate (Figure 3A). The in-situ growth of $CsPbBr_3$ nanostructures on the nanoplate template was further confirmed by green emission after 365 nm excitation, which coincided with the red upconversion emission from nanoplates (Figure 3B).

We next examined the formation of perovskite nanostructures on the $CsYb_2F_7$ nanoplate by high-resolution electron microscopy. High-angle annular dark-field (HAADF) imaging showed that crystal lattice sites on the (001) facet of the $CsYb_2F_7$ nanoplate became brighter after the reaction, indicating successful growth of Pb^{2+} ions (Figure 3C,D). It is noteworthy that the structure determined by electron microscopy agrees well with the modeling, showing that the (111) facet of the $CsPbBr_3$ nanostructure is firmly docked to the (001) facet of the nanoplate (Figure 3E). $CsPbBr_3$ reconstruction on the $CsYb_2F_7$ nanoplate is likely enabled by the minimal lattice mismatch (<5%) between these two facets.[10] Extended X-ray absorption fine structure (EXAFS) was further used to probe the coordination environment surrounding Yb^{3+} in $CsYb_2F_7$ and $CsYb_2F_7/CsPbBr_3$ (Table S2 and Figure S10, Supporting Information). EXAFS spectra fitting results showed that the surface growth of $CsPbBr_3$ on $CsYb_2F_7$ leads to a slight alteration in the coordination number of Yb^{3+} ions, increasing from 6.7 to 6.9. This suggests that the growth of surface perovskites has

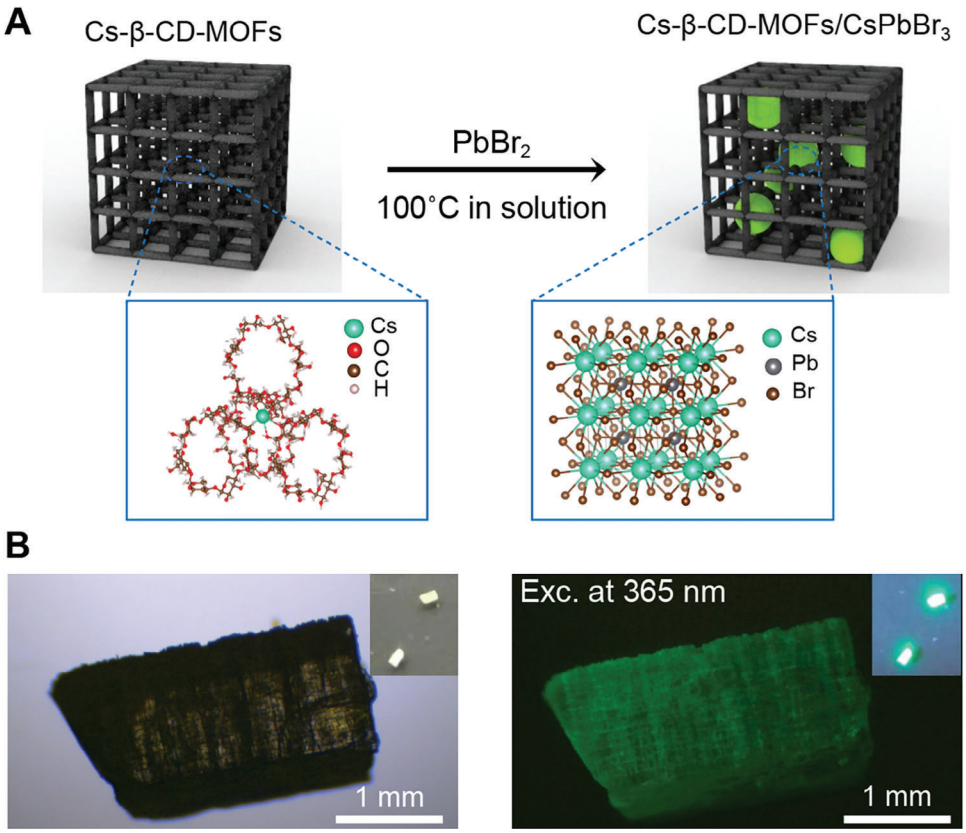

Figure 5. Conversion of Cs-β-CD-MOFs to bright Cs-β-CD-MOFs/$CsPbBr_3$ hybrids. A) Schematic illustration of the Cs^+-MOF to MOF/Perovskite conversion process. The two 3D frames indicate the crystal structures of the Cs-β-CD-MOFs (left) and Cs-β-CD-MOFs/$CsPbBr_3$ composite (right). B) Images of Cs-β-CD-MOFs/$CsPbBr_3$ composite under ambient light (left) and 365 nm UV stimulation (right).

a limited impact on the inner coordination characteristics. It is conceivable that the different exposure of the Cs^+ sublattice at each facet of the sub-10 nm $CsYb_2F_7$ nanoplatform could lead to varying degrees of versatility in the nucleation and growth of perovskites, as reflected in the occurrence of multiple emission bands as a result of exciton confinements to different extents.

To further explore the potential of this strategy in controlling perovskite growth and exciton confinement, we synthesized $CsYb_2F_7$ nanoplates with much lower homogeneity to expose as many crystal facets as possible for the subsequent preparation of lead-halide perovskites. Compared with products obtained with uniform $CsYb_2F_7$ nanoparticles of size sub-10 nm, two additional excitonic transition bands, blue-shifted to 402 nm, were observed (**Figure** 4A). It should be noted that the peak positions of these emission bands are consistent with those of reported low-dimensional perovskite nanomaterials, suggesting success in molecular-level engineering of perovskite nanostructures using the Cs^+-sublattice platform.[11] Moreover, the strong quantum confinement enhances the interaction between the excitons and the surrounding environment, leading to increased nonradiative recombination and drastic luminescence lifetime decline from 8 to 1 ns (Figure 4B). We also found that this new strategy is applicable when switching from bromide to other halides. This allows lead-halide perovskites with a wide spectral coverage from blue to deep red with no discernible difference for XRD after reaction using a homogeneous nanorod platform (Figure 4C; Figure S11–S15, Supporting Information). A high quantum yield of ≈86% was measured for as-synthesized $CsPbBr_3$ nanostructures (Figure S16, Supporting Information). Interestingly, the $CsPbBr_3$ nanostructures prepared on the rigid Cs^+-sublattice nanoplatform show significantly improved water resistance compared to their counterparts prepared by conventional methods. When 5% water by volume was added to a cyclohexane solution of perovskite nanomaterials, more than 60% of the original intensity was retained after 30 min, while the $CsPbBr_3$ QDs lost 90% of their original intensity in less than 10 min (Figure 4D).

Importantly, we demonstrated that in-situ growth of highly luminous green-emitting perovskites on a single crystal of a Cs-based cyclodextrin (CD) metal-organic framework (MOF) known as Cs-β-CD-MOF. This achievement underscores the versatility and reliability of the approach for the development of hybrid functional nanosystems (**Figure** 5).

3. Conclusion

Thus, by employing an ion-enriched crystalline nanoplatform to control the synthesis kinetics precisely, we have developed a new strategy for preparing MHP nanostructures with tunable luminescence and improved stability. Our study indicates that the abundant crystal facet exposure of the Cs^+-preconfined nanoplatform can effectively impart different growth kinetics to

the perovskite structure, resulting in varying degrees of exciton confinement and consequently multiple emission bands. While beam-sensitive material-friendly electron microscopy techniques are still needed to fully probe the nature of perovskite nucleation and growth on each facet, we believe that this strategy opens up a new avenue for creating high-quality functional nanostructures. This development provides new opportunities for nanophotonics, quantum optics, energy conversion, and numerous other applications. We also speculate that this strategy could provide new insights for areas, such as atomic-scale nanocrystal engineering and the control of excitonic transitions.

Supporting Information

Supporting Information is available from the Wiley Online Library or from the author.

Acknowledgements

This work was supported by the Singapore Ministry of Education (MOE2017-T2-2-110, MOE2016-T3-1-006 (S)), Agency for Science, Technology and Research (A*STAR) (A1983c0038), and National Research Foundation, Prime Minister's Office, Singapore under the NRF Investigatorship programme (Award No. NRF-NRF105-2019-000, NRF-CRP18-2017-023, and NRF-CRP19-2017-01).

Conflict of interest

The authors declare no conflict of interest.

Data Availability Statement

The data that support the findings of this study are available in the supplementary material of this article.

Keywords

exciton confinement, growth kinetics, metal-halide perovskite, metal-organic framework, sublattice

Received: September 12, 2023
Revised: October 27, 2023
Published online: November 28, 2023

[1] a) Y. Chen, J. Yin, Q. Wei, C. Wang, X. Wang, H. Ren, S. F. Yu, O. M. Bakr, O. F. Mohammed, M. Li, *Nat. Photonics* **2022**, *16*, 485; b) R. Sun, D. L. Zhou, Y. J. Ding, Y. Wang, Y. Q. Wang, X. M. Zhuang, S. A. Liu, N. Ding, T. Y. Wang, W. Xu, H. W. Song, *Light Sci. Appl.* **2022**, *11*, 340; c) Y. Wei, K. Li, Z. Cheng, M. Liu, H. Xiao, P. Dang, S. Liang, Z. Wu, H. Lian, J. Lin, *Adv. Mater.* **2019**, *31*, 1807592; d) H. Zhu, Y. Pan, C. Peng, H. Lian, J. Lin, *Angew. Chem., Int. Ed.* **2022**, *61*, e202116702; e) J. S. Kim, J.-M. Heo, G.-S. Park, S.-J. Woo, C. Cho, H. J. Yun, D.-H. Kim, J. Park, S.-C. Lee, S.-H. Park, E. Yoon, N. C. Greenham, T.-W. Lee, *Nature* **2022**, *611*, 688; f) X.-K. Liu, W. Xu, S. Bai, Y. Jin, J. Wang, R. H. Friend, F. Gao, *Nat. Mater.* **2021**, *20*, 10; g) X. Li, F. Cao, D. Yu, J. Chen, Z. Sun, Y. Shen, Y. Zhu, L. Wang, Y. Wei, Y. Wu, H. Zeng, *Small* **2017**, *13*, 1603996; h) M. V. Kovalenko, L. Protesescu, M. I. Bodnarchuk, *Science* **2017**, *358*, 745; i) Y. Liu, Y. Dong, T. Zhu, D. Ma, A. Proppe, B. Chen, C. Zheng, Y. Hou, S. Lee, B. Sun, E. H. Jung, F. Yuan, Y.-K. Wang, L. K. Sagar, S. Hoogland, F. P. García De Arquer, M.-J. Choi, K. Singh, S. O. Kelley, O. Voznyy, Z.-H. Lu, E. H. Sargent, *J. Am. Chem. Soc.* **2021**, *143*, 15606.

[2] a) K. Lee, M. Kim, H. Kim, *J. Mater. Chem.* **2010**, *20*, 3791; b) Y.-M. Chen, Y. Zhou, Q. Zhao, J.-Y. Zhang, J.-P. Ma, T.-T. Xuan, S.-Q. Guo, Z.-J. Yong, J. Wang, Y. Kuroiwa, C. Moriyoshi, H.-T. Sun, *ACS Appl. Mater. Interfaces* **2018**, *10*, 15905; c) J. Shamsi, A. S. Urban, M. Imran, L. De Trizio, L. Manna, *Chem. Rev.* **2019**, *119*, 3296; d) Q. Fan, G. V. Biesold-Mcgee, J. Ma, Q. Xu, S. Pan, J. Peng, Z. Lin, *Angew. Chem., Int. Ed.* **2020**, *59*, 1030; e) M. Imran, L. Peng, A. Pianetti, V. Pinchetti, J. Ramade, J. Zito, F. Di Stasio, J. Buha, S. Toso, J. Song, I. Infante, S. Bals, S. Brovelli, L. Manna, *J. Am. Chem. Soc.* **2021**, *143*, 1435.

[3] a) D. W. Duan, C. Y. Ge, M. Z. Rahaman, C. H. Lin, Y. M. Shi, H. R. Lin, H. L. Hu, T. M. Wu, *NPG Asia Mater* **2023**, *15*, 8; b) Q. A. Akkerman, T. P. T. Nguyen, S. C. Boehme, F. Montanarella, D. N. Dirin, P. Wechsler, F. Beiglböck, G. Rainò, R. Erni, C. Katan, J. Even, M. V. Kovalenko, *Science* **2022**, *377*, 1406; c) M. J. Ashley, M. N. O'brien, K. R. Hedderick, J. A. Mason, M. B. Ross, C. A. Mirkin, *J. Am. Chem. Soc.* **2016**, *138*, 10096; d) S. Bera, S. Shyamal, N. Pradhan, *J. Am. Chem. Soc.* **2021**, *143*, 14895.

[4] Y. Wei, Z. Cheng, J. Lin, *Chem. Soc. Rev.* **2019**, *48*, 310.

[5] Y. Jiang, C. Sun, J. Xu, S. Li, M. Cui, X. Fu, Y. Liu, Y. Liu, H. Wan, K. Wei, T. Zhou, W. Zhang, Y. Yang, J. Yang, C. Qin, S. Gao, J. Pan, Y. Liu, S. Hoogland, E. H. Sargent, J. Chen, M. Yuan, *Nature* **2022**, *612*, 679.

[6] C. Tan, J. Chen, X.-J. Wu, H. Zhang, *Nat. Rev. Mater.* **2018**, *3*, 17089.

[7] a) P. Pei, Y. Chen, C. Sun, Y. Fan, Y. Yang, X. Liu, L. Lu, M. Zhao, H. Zhang, D. Zhao, X. Liu, F. Zhang, *Nat. Nanotechnol.* **2021**, *16*, 1011; b) F. Wang, Y. Han, C. S. Lim, Y. Lu, J. Wang, J. Xu, H. Chen, C. Zhang, M. Hong, X. Liu, *Nature* **2010**, *463*, 1061.

[8] a) J. Zhu, S. Wang, Z. Yang, S. Liao, J. Lin, H. Yao, F. Huang, Y. Zheng, D. Chen, *Nanoscale* **2022**, *14*, 3407; b) H. Schafer, P. Ptacek, H. Eickmeier, M. Haase, *J. Nanomater.* **2009**, *2009*, 685624.

[9] a) X. Guan, Z. Lei, X. Yu, C.-H. Lin, J.-K. Huang, C.-Y. Huang, L. Hu, F. Li, A. Vinu, J. Yi, T. Wu, *Small* **2022**, *18*, 2203311; b) Y. Bekenstein, B. A. Koscher, S. W. Eaton, P. Yang, A. P. Alivisatos, *J. Am. Chem. Soc.* **2015**, *137*, 16008; c) J. Xing, Y. Zhao, M. Askerka, L. N. Quan, X. Gong, W. Zhao, J. Zhao, H. Tan, G. Long, L. Gao, Z. Yang, O. Voznyy, J. Tang, Z.-H. Lu, Q. Xiong, E. H. Sargent, *Nat. Commun.* **2018**, *9*, 3541.

[10] Y. Wang, F. Yang, X. Li, F. Ru, P. Liu, L. Wang, W. Ji, J. Xia, X. Meng, *Adv. Funct. Mater.* **2019**, *29*, 1904913.

[11] a) N. Yantara, N. F. Jamaludin, B. Febriansyah, D. Giovanni, A. Bruno, C. Soci, T. C. Sum, S. Mhaisalkar, N. Mathews, *ACS Energy Lett.* **2020**, *5*, 1593; b) G. Almeida, L. Goldoni, Q. Akkerman, Z. Dang, A. H. Khan, S. Marras, I. Moreels, L. Manna, *ACS Nano* **2018**, *12*, 1704.

